Engineering and Technology Journal
Journal homepage: https://etj.uotechnology.edu.iq

Air-lift Reactor's Characterization via Computational Fluid Dynamic (CFD): Review

Marwa M. Jasim*, Thamer J. Mohammed, Laith S. Sabri

Chemical Engineering Dept., University of Technology-Iraq, Alsina'a Street,10066 Baghdad, Iraq.
*Corresponding author Email: che.19.20@grad.uotechnology.edu.iq

HIGHLIGHTS

- Many CFD models for Air-lift reactors are reviewed.
- Flow regime, bubble properties, and hydrodynamics characteristics are covered.
- Available closure correlations are investigated.

ARTICLE INFO

Handling editor: Qusay F. Alsalhy
Keywords:
Computational fluid dynamics
air-lift reactor
review

ABSTRACT

Airlift reactors are seen as the most promising reactor for many valuable productions such as algae culturing. However, this kind of reactor still needs more information and data to understand its phenomena due to limited studies. Also, to reduce the time and offers obtained with sufficient reactor design, capable of achieving high productivities, Computational Fluid Dynamics (CFD) could play an important role in optimizing the reactor design by analyzing the interaction of hydro-dynamics. This review presents the literature review on the recent CFD work for such a reactor that addressed the fluid dynamics parameters, such as bubble dynamics. Earlier researches find more reports utilizing uniform bubble diameter in CFD simulations. However, the latest research in the CFD modeling of multi-phase flow reactors showed that the description of the bubble has significant effects on the performance of the simulation. As a result, systematic research into the impact of bubble diameter on the simulation results of the CFD was performed. Finally, we present and discuss the CFD modeling approaches, a Governing equation such as Eulerian-Eulerian (E-E), and closure such as the drag force.

1. Introduction

Pneumatically agitated vessels, known as airlift reactors, are one of many types of multi-phase reactors. Airlift reactors are commonly utilized in the chemical, environmental, petro-chemical, and bio-process industries, including fermentations [1] and waste-water treatments [2]. Airlift reactors are gaining popularity in chemical engineering because of their numerous benefits, including sufficient mass and heat transfer, low-pressure drop, and high fluid circulation rate. As a result, there aren't any moving parts in airlift reactors. In contrast to the mechanically stirred tank reactors and bubble column reactors [3, 4]. The airlift reactor may be operating at higher gas throughputs and achieving sufficient wall heat transfer and mixing compared with the traditional bubble column [5]. The loop reactors are utilized in bio-chemical applications because they have a low degree of shear stress, allowing micro-organisms to expand rather than break down in high shear stresses. Airlift column reactors have recently been recognized as having the potential to dramatically boost the capability of the photo-synthetic micro-organisms in using light energy with a higher effectiveness, thus enhancing the general efficiency of the culturing system due to their high mixing rate [6-8]. A wide range of applications of ALR has resulted in a multitude of studies in recent decades, focusing on their flow dynamic characteristics and simulation [9, 10], reactor adjustment [11-13], and geometry optimization [14]. The hydro-dynamic behaviors and the mixing properties that are crucial parameters for designing the airlift reactors, operation, and scaling up may be utilized to define the efficiency of airlift reactors generally [15].

The mixing properties are usually based on circulation time, axial dispersion coefficient mixing time, and the axial dispersion number. In contrast, hydro-dynamic behaviors are usually described in gas velocity, liquid velocity, and gas hold-up. Those mixing and hydro-dynamic parameters, like the gas sparger type, superficial gas velocity, ratio height-to-riser-diameter, downcomer diameter, and scale-up, depending on operating parameters. Numerous researches focused on the experimental investigations of hydrodynamics in a global gas hold-up form and velocity in riser and downcomer [16,17]. There has also been literature concerning the local hydro-dynamics for the liquid velocity and gas hold-up in internal loop airlift

http://doi.org/10.30684/etj.v40i3.2261
Received 26 June 2021; Accepted 27 October 2021; Available online 25 March 2022
2412-0758/University of Technology-Iraq, Baghdad, Iraq

reactors [18-23], using the CARPT for testing local liquid velocity and gas hold-up. With the technical development of airlift reactors in recent decades, have developed CFD simulations as one of the generally adopted numerical techniques for studying local properties (such as profiles of gas hold-up, liquid velocity profiles, and shear stress profiles) of multi-phase flow dynamics in airlift column reactors [24]. Several researchers have created the CFD model for gas-liquid flow in air-lift reactors. In addition, as shown in Appendix, they used various turbulent and geometrical models for simulations of gas-liquid flow in airlift reactors. Numerous researches on hydro-dynamics in the IALR based upon the simulation of the CFD [25, 26] evaluated the capability of CFD simulation to capture global flow concerning the interstitial velocity and gas hold-up in internal loop airlift reactors. Huang et al. (4) Have simulated hydro-dynamics and mass transfer in axisymmetric IALR using a steady 2-fluid model; they have been focused upon global hold-up of gas, mass transfer coefficient liquid velocity. The majority of research in this field was dependent upon the 2-D geometry or the axisymmetric assumption, but 3-D transient simulations are required to capture the real flow within the system and investigate the reactor's mixing patterns.

Despite the increased interest in hydro-dynamic research, only a small number of the studies on the residence and mixing time were found to be investigated in terms of the mixing and residence times for external loop reactors. Those parameters of mixin ando the others like the dispersion, circulation time, etc., have been researched. The RTD with the tracer method may be utilized to obtain the information, with obtaining the RTD curve by monitoring the concentration of the outlet over time. To obtain mixing parameters, RTD is also required to match proper phenomenological models. In the airlift reactors, the axial dispersion model had been primarily utilized as a model of mixing [27]. Roy et al. [28] simulated flow field, axial dispersion coefficient, and mixing time in an external loop air-lift reactor. They have focused on hydro-dynamics and mixing in a reactor's riser of the liquid phase. Beihin et al. [27] have utilized mathematical modeling combined with the experimental data to characterize the mixing in a concentric double-draft tube. Circulation time and mixing time were utilized for characterizing the properties of the liquid mixing. The majority of the literature on the subject was focused on the liquid phase mixing in a system. In addition, the values of axial dispersion coefficient in parts of the riser and the downcomer of air-lift reactors can differ [3]. Olaofe et al. [28] have shown that computational mixing research using the virtual tracer simulation approach is an effective tool for understanding multi-phase reactors. Unlike experimental research, simulation research does not require expensive tools, and geometrical effects may be studied easily because no new equipment is required. This review aims to provide a thorough overview of CFD modeling techniques, which include a multi-phase flow structure model, bubble descriptions, and easily accessible closure correlations. This review presents a detailed overview of these efforts, which will aid ALR researchers in quickly mastering existing information and, more importantly, analyzing current gaps or defects and stimulating or evoking some novel thinking in this area.

2. Analyses of Flow Dynamic Characteristics in Air-Lift Reactor

Generally, the ALRs can be observed as traditional bubble column reactors (BCR) modified by in-built baffles. The usual ALR can be divided into 4 distinctive hydro-dynamic zones or sections: riser (i.e., draft tube), bottom clearance, downcomer, and gas separation (de-gassing) part. State-of-the-art structures of the reported typical ALR have been illustrated in Figure 1. Based on the layout of those areas, the ALRs are usually categorized into 2 types: internal (IL-ALR) and external loop ALR (EL-ALR). The IL-ALR consists of coaxial concentric tubes or baffle-split vessels. Coaxial concentric tube ALRs may be running at 2 separate modes, referred to as the perimeter aeration ALR (referred to as inverse ALR) and center aeration ALR as shown in Figure 1. Due to the neigh-boring location of a riser and downcomer, a large quantity of the bubbles that enter the de-gassing section from the riser can be entrained easily by the flow of the downcomer.

In contrast, EL-ALR includes 2 separate tubes that are only connected at the bottom and top sections of the ALR. Due to a rather long distance of riser-downcomer, a small number of the bubbles have been entrapped by the flow of the downcomer [29]. The ALR's geometry makes the pattern of the flow more organized in comparison with the BCR: disordered flows in BCR are substituted by ones that are ordered in an almost vertical orientation, which makes the ALRs with a higher efficiency to utilize buoyancy, incident kinetic energy, isotherm expansion energy of the rising bubbles—as a result, enhancing the level of energy efficiency. Despite various ALR geometries, there remains some similarity in the properties of the flow dynamics.

Nonetheless, the flow properties differ considerably in sections of ALR: every one of the sections has different characteristics of the local flow in momentum, heat, and mass transfer [30]. The diverged flow properties in the sections ensure certain ALR functions are improved in certain applications. For instance, Li et al. [31] have noted significant nitrogen removal with simultaneous nitrification and denitrification (SND) in ALRs. They have shown that gradient distribution of the DO (i.e., dissolved oxygen) imposed a considerable impact on the SND. Wei & Zhang [32] have accomplished the removal of biological nitrogen using the SND process in bench-scale IL-ALR, where riser played the nitrification zone, and down-comer has been utilized for the denitrification. A similar removal of the nitrogen using the SND in the downcomer has been explained by Meng et al. [33, 34] and Meng et al. [35].

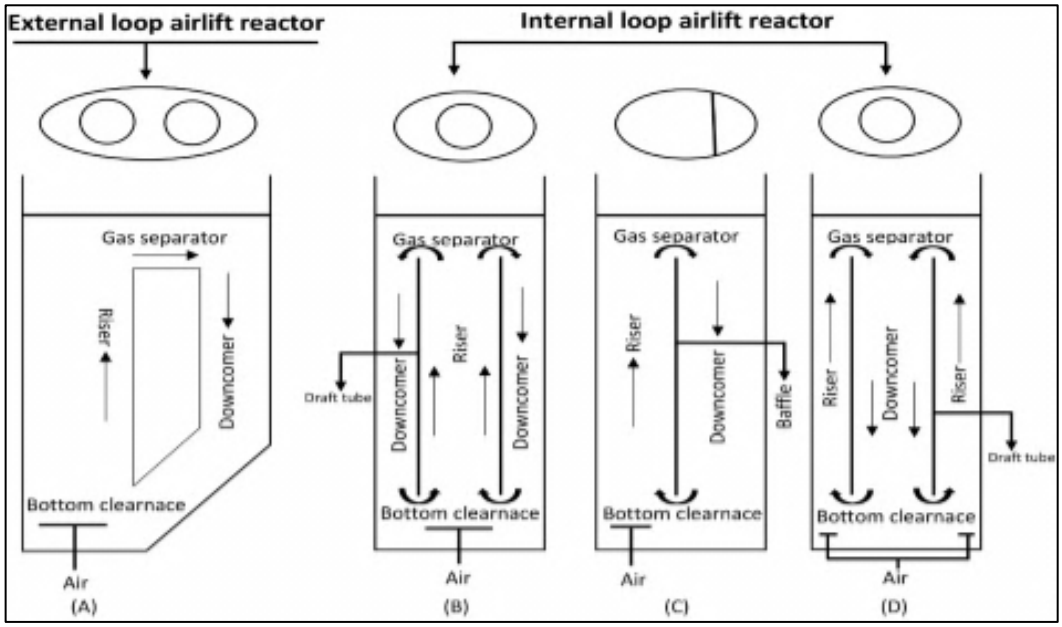

Figure 1: Structural schematic of typical ALRs: (A) External loop ALR (B) Center aeration ALR (C) Baffle-split vessels (D) Perimeter aeration ALR

3. CFD-Based Models

CFD has the best potential for long-term applications amongst the numerous models utilized to predict hydro-dynamics and associated properties of the PBR and other multi-phase flow systems [36, 37]. CFD is a useful method for analyzing fluid flows. This tool solves problems concerning fluid movement with the aid of computers and computational techniques. A numerical model representing a system or device may be developed using the CFD, and the fluid dynamics and associated physical phenomena may be predicted using the fluid flow physics and chemistry applied to this virtual model. Inside every one of the cells of the computational domain, Navier–Stokes equations are numerically solved using the CFD technique. CFD is thought to be a valuable method for supplementing the limitations of field and laboratory studies and a low-cost solution. CFD may be utilized to investigate the ALRS affecting hydro-dynamics of flow, for example, the gas hold-up, superficial gas velocity, column geometry, bubble diameter, pressure, and antifoaming content, all of which are all factors that significantly impact liquid currents in a column. Liquid currents are difficult to predict since predicting the air-lift reactor hydro-dynamics in the lab experimentations is hard. Due to the increase in the capability and affordability of computers, the applications of the CFD to the design of the ALR are becoming more common, allowing for faster computation times and the ability to solve even the most complex geometry. Numerous promising works in CFD modeling of ALRs have been carried out over the last decade, showing that it is an effective and indispensable tool to study optimization and scale-up. The new advances in the CFD modeling of ALRs were studied [38-40]. Comparisons showed that the algorithm performance, as shown in Figure 2, depends on the flow states and the extent of paired between the numerical equations and the momentum and occasionally even on the numerical approach details utilized in solving the algebraic equations. The finite volume approach begins with the flow domain discretization and the corresponding transport equations. Then discretized momentum equations are solved by the guessed field of pressure to give the components the velocity of (v_r* and v_x*) as follows:

$$a_{i,j}\, v_{r\ i,j}^{*} = \sum a, v_r^{*} + \left(p_{i-1}^{*} - p_{i,j}^{*}\right)A_{I,J} \quad (1)$$

$$a_{i,j}\, v_{x\ i,j}^{*} = \sum a, v_x^{*} + \left(p_{1,j-1}^{*} - p_{i,j}^{*}\right)A_{I,J} \quad (2)$$

$$a_{i,j}p'_{i,j} = a_{i+1,j}p'_{i+1,j} + a_{i-1,j}p'_{i-1,j} + a_{i,j+1}p'_{i,j+1} + a_{i,j-1}p'_{i,j-1} + b'_{ij} \quad (3)$$

$$\text{Correct } V_r \,\&\, V_x = \text{initial velocity} + \text{av}^{*}(\text{v from eq. (1) \& (2)}) \quad (4)$$

$$\text{Correct p} = \text{initial pressure} + \text{ap}^{*}(\text{p from eq. (3)}) \quad (5)$$

Moreover, the accuracy of CFD predictions is currently dependent on CFD models, sub-models, and closure equations that describe the phenomena of flow.

To summarize, recent ALR CFD modeling efforts have focused on two key aspects:

1. Selecting appropriate models for multi-phase flow.
2. Establishing closure relationships for interphase in- interaction and turbulence of the fluid.

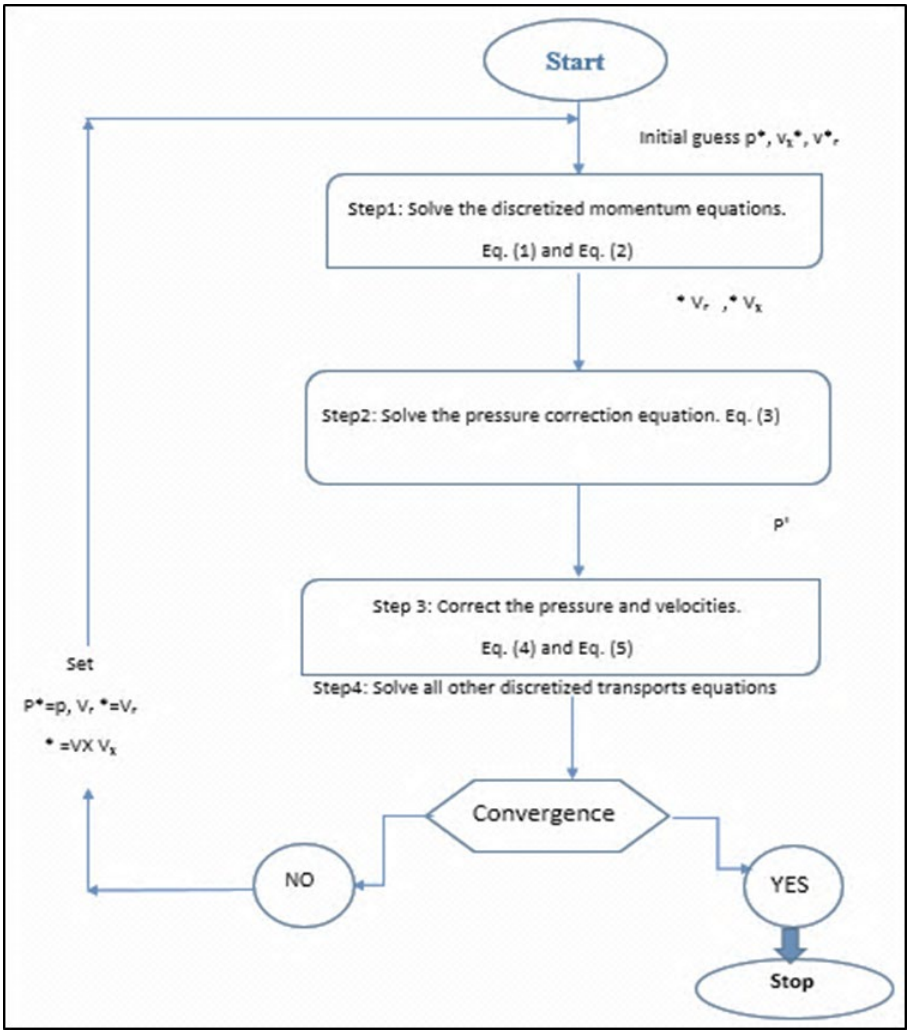

Figure 2: The SIMPLE algorithm flow chart

3.1 Multi-Phase Flow Models

3.1.1 Framework Model Approach

In ALR's CFD simulation, liquids are typically considered background fluids, which is referred to as the continuous or primary phase. The gas and potential solids are usually treated as particulate phases dispersed in background fluid, referred to as the dispersed phases. Almost all related publications follow the continuous step using the Eulerian framework model system. The Eulerian and the Lagrangian tracking methods are used to monitor the dispersed process. The Eulerian approach employs a stationary coordinate approach to define the flow parameter distribution in the flow region. The Lagrangian approach utilizes a moving coordinate scheme to map each particle's movement trajectories, summing up particle movement to the flow field's flow properties. The Eulerian-Eulerian (E-E) and Eulerian-Lagrangian (E–L) models are 2 combined structure models that are utilized in the simulations of the CFD of gas-liquid-solid and gas-liquid multi-phase flow in ALR [25]. The latter is used to treat the continuous and scattered liquids as inter-penetrating liquids with a unity volume fraction restriction, with momentum conservation and separated mass equations describing all phase's flow. Interactions between the phases are combined with the addition of the source items at the conservation equations' right side, describing the momentum and mass transfer between any 2 phases. Dispersed phases can be solved by monitoring numerous bubbles or particles through a measured flow area.In contrast, the liquid phase has been viewed as a continuum through a solution of time-averaged Navier-Stokes equations. The dispersed phase may be exchanging the momentum and the mass with continuous phases. However, the primary phase's flow field calculations have not considered its effects on the continuous phases. E–L approach is advantageous in tracking the movements of any particles whenever desired. The E–L model makes it reasonably simple to incorporate bubble and particle coalescence, breakup, and collisions [41]. The E–L process, on the other hand, needs a lot of resources to determine the trajectory of each particle individually.Consequently, where the movement of a single particle is required, and the entire number of the considered particles has been found limited, the E–L approach is frequently used. On the other hand, even though the E-E method can only provide a spatial distribution of the flow parameters, its measurement requirements are lower, allowing for more flexibility in terms of the number and volume fraction of dispersed phases. E-E models, known as 2-fluid models, have been more popular than the E–L models. Utilizing the 2-fluid model, a steady-state simulation of the CFD for IL-ALR operates at low SVG's. Baten et al. [42] compared experimental findings against the hydrodynamics modeling in IL-ALRs of 2 configurations using CFD. Volume-averaged mass and the momentum conservation Eqs. In Eulerian system has been utilized in their CFD models for both water and air phases. Huang et al. [43] provided a 3-D IL-ALR simulation for the 2-

phase bubbly flow using the 2-fluid model with revise k –ε turbulence model. Pawar [44] used 2-phase CFD simulations with the E–L method to investigate the flow dynamics of a concentric tube ALR, where the water has been in a continuous phase with the dispersed air. The separate bubbles have been monitored from sparger at a point of injection to the top of the reactor, where they escaped. In this study, 2 different BSDs (i.e., bubble size distributions) and their Sautermean diameter were considered to represent the gas distribution at sparger in the reactor. The present paper shows that BSD-1 (1mm–5mm–10mm) that contains a high fraction of the small bubbles (less than 5mm) appropriately represents the flow hydro-dynamics in comparison with BSD-2 (5mm–10mm–15mm) that contains a high portion of the large bubbles (more than 10mm) or single size bubble diameter (5.25mm and 10mm). In addition to that, 3 operation regimes, like, no gas bubbles in downcomer (regime I), stationary gas bubbles in downcomer (regime II), and re-circulation of the gas bubbles from downcomer to riser sections (regime III) have been verified by the use of the CFD simulations with the Lagrangian particle tracking. Satisfactory agreements (in approximately 15% deviation) with experimental data have been noticed for some parameters like gas hold-ups in riser and down-comer and liquid circulation velocity inflow regimes I & II for BSD-1.

3.2 Multi-Phase Flow Models

3.2.1 Framework Model Approach

In ALR's CFD simulation, liquids are typically considered background fluids, which is referred to as the continuous or primary phase. The gas and potential solids are usually treated as particulate phases dispersed in background fluid, referred to as the dispersed phases. Almost all related publications follow the continuous step using the Eulerian framework model system. The Eulerian and the Lagrangian tracking methods are used to monitor the dispersed process. The Eulerian approach employs a stationary coordinate approach to define the flow parameter distribution in the flow region. The Lagrangian approach utilizes a moving coordinate scheme to map each particle's movement trajectories, summing up particle movement to the flow field's flow properties. The Eulerian-Eulerian (E-E) and Eulerian-Lagrangian (E–L) models are two combined structure models that are utilized in the simulations of the CFD of gas-liquid-solid and gas-liquid multi-phase flow in ALR [25]. The latter is used to treat the continuous and scattered liquids as inter-penetrating liquids with a unity volume fraction restriction, with momentum conservation and separated mass equations describing all phase's flow. Interactions between the phases are combined with the addition of the source items at the conservation equations' right side, describing the momentum and mass transfer between any 2 phases. Dispersed phases can be solved by monitoring numerous bubbles or particles through a measured flow area.In contrast, the liquid phase has been viewed as a continuum through a solution of time-averaged Navier-Stokes equations. The dispersed phase may be exchanging the momentum and the mass with continuous phases. However, its effects on the continuous phases have not been considered in the primary phase's flow field calculations. E–L approach is advantageous in tracking the movements of any particles whenever desired. The E–L model makes it reasonably simple to incorporate bubble and particle coalescence, breakup, and collisions [41]. The E–L process, on the other hand, needs a lot of resources to determine the trajectory of each particle individually. Consequently, where the movement of a single particle is required, and the entire number of the considered particles has been found limited, the E–L approach is frequently used. On the other hand, even though the E-E method can only provide a spatial distribution of the flow parameters, its measurement requirements are lower, allowing for more flexibility in terms of the number and volume fraction of dispersed phases. E-E models, known as 2-fluid models, have been more popular than the E–L models. Utilizing the 2-fluid model, a steady-state simulation of the CFD for IL-ALR operates at low SVG's. Baten et al. [42] compared experimental findings against the hydrodynamics modeling in IL-ALRs of 2 configurations using CFD. Volume-averaged mass and the momentum conservation Eqs. In Eulerian system has been utilized in their CFD models for both water and air phases.Huang et al. [43] provided a 3-D IL-ALR simulation for the 2-phase bubbly flow using the 2-fluid model with a revised k –ε turbulence model. Pawar [44] used 2-phase CFD simulations with the E–L method to investigate the flow dynamics of a concentric tube ALR, where the water has been in a continuous phase with the dispersed air. The separate bubbles have been monitored from sparger at a point of injection to the top of the reactor, where they escaped. In this study, 2 different BSDs (i.e. bubble size distributions) and their Sautermean diameter were considered to represent the gas distribution at sparger in the reactor. The present paper shows that BSD-1 (1mm–5mm–10mm) that contains a high fraction of the small bubbles (less than 5mm) appropriately represents the flow hydro-dynamics in comparison with BSD-2 (5mm–10mm–15mm) that contains a high portion of the large bubbles (more than 10mm) or single size bubble diameter (5.25mm and 10mm). In addition to that, 3 operation regimes, like, no gas bubbles in downcomer (regime I), stationary gas bubbles in downcomer (regime II), and re-circulation of the gas bubbles from downcomer to riser sections (regime III) have been verified by the use of the CFD simulations with the Lagrangian particle tracking. Satisfactory agreements (in approximately 15% deviation) with experimental data have been noticed for parameters like gas hold-ups in riser and down-comer and liquid circulation velocity in flow regimes I & II for BSD-1.

3.1.1.1. Governing Equation

In the Euler-Euler methodology, the two phases have been treated as inter-penetrating fluids' continua. Ensemble-averaged equations of mass and momentum conservations are utilized to describe the two phases' time-dependent motions. The ensemble-averaged terms of interaction that describe drag, lift force, and virtual mass effects appear in the momentum balances of the 2 phases [45].

Continuity equation: -

$$\frac{\partial}{\partial t}(\rho_k \varepsilon_k) + \nabla(\rho_k \varepsilon_k u_k) = 0 \quad (6)$$

Momentum transfer equation: -

$$\frac{\partial}{\partial t}(\rho_k \varepsilon_k u_k) + \nabla(\rho_k \varepsilon_k u_k u_k) = -\nabla(\varepsilon_k \tau_k) - \varepsilon_k \nabla p + \varepsilon_k \rho_k g + M_{g,l} \quad (7)$$

In Euler-Lagrange representation, individual bubbles have been separately tracked, whereas liquid has been treated as a continuum. The motion of the bubble is described by Newtonian laws, which offer the benefit of the simple implementation of forces that have been exerted on the bubbles. The variety of the equations that have been utilized in the CFD model to solve the Momentum and mass balances for the liquid phase can be summarized below. For the Newtonian fluid, incompressible, isothermal, and unsteady state [44].

Equation of Continuity: -

$$\frac{\partial \rho}{\partial t} + \nabla.(u) = 0 \quad (8)$$

Momentum transfer equation: -

$$\frac{\partial(\rho u)}{\partial t} + \nabla(\rho u u) = -\nabla p + \rho.g + \nabla\left(\mu_{eff}\left(\nabla U + (\nabla U)^T\right)\right) + M_{g.l} \quad (9)$$

Where: U: represents averaged liquid phase velocity; g: represents the vector of gravity; p: represents pressure; ρ : represents liquid phase density; μ_{eff} : represents the liquid phase's effective viscosity, $M_{g,l}$: represents interfacial momentum forces in governing momentum equation9 are responsible for interactions between dispersed and continuous phases.

3.2.2 Bubble Dynamic

To simplify CFD modeling, gas bubbles in ALRs are assumed to have a constant uniform diameter. The equivalent average diameter of the bubble derived from the experimental measurements has been typically utilized to calculate the diameter of the bubble for the CFD modeling. However, a randomly designated bubble diameter is typically selected to match experimental data. For instance, Al-Dahhan & Luo [20] simulated the local flow dynamics' CFD in the draft tube air-lift bio-reactor, where gas bubbles have been considered to have a diameter of 3mm. Their model of the CFD reasonably predicted the re-circulation of the micro-organisms compared to tracer trajectories that have been experimentally measured. Sufficient results have been obtained from the relatively low SGV, which makes flow behave in a homogeneous flow pattern of the bubbles. Earlier research [46-48] finds more reports utilizing uniform bubble diameter in CFD simulations. The latest research in the CFD modeling of multi-phase flow reactors showed that the description of the bubble has significant effects on the performance of the simulation [49-50]. As a result, systematic research into the impact of bubble diameter on the simulation results of the CFD was performed. Mohajrani et al. [51] investigated the impacts of the bubble diameter from (1mm - 9mm) in 2-phase ALRs of 3 distinct configurations, finding that the smaller diameters of the bubble had a higher aspect ratio of the bubble, which has resulted in a decreased liquid velocity and gas hold-up. Huang et al. [4] used a steady Reynolds averaging 2-fluid model to examine the bubbly flow's sensitivity in an IL-ALR. The effects of the bubble size on simulation results were evaluated in the range of (2 - 10) mm, demonstrating its importance in effective simulation. For bubbly flow with many different bubble sizes, a multiple size group (MUSIG) model has been proposed as a pre-requisite for quality modeling. Indeed, bubbles of various sizes and shapes can be found in gas-liquid or gas-liquid-solid dispersions in most industrial reactors, particularly at high SGV. The shapes and the sizes of bubbles impact phase velocity and volume fraction distribution, and the phase velocity and volume fraction distribution impact the shapes and the sizes of bubbles as well [52]. Some research discarded the assumption of the uniform constant bubble diameters in favor of the MUSIG bubble representation model to obtain a more precise simulation performance. MUSIG models, such as (PBM) and (DBS), were successfully used to simulate ALR flow dynamics. The DBS model for gas-liquid flows is mainly an extension of the method of the (EMMS) that has been developed by [53]. This model divides heterogeneous gas-liquid flow structure into the liquid phase, and 2 bubble groups, $d_{L,}$ and d_S, are described based on their equivalent bubble diameter values. The small and large bubbles share one liquid flow area, and their interfaces interact with the surrounding liquid. The energy consumption was partitioned into micro and meso-scale sections using force balance and mass equations for the two bubble sizes. Six structural parameters, including d_S and d_L, f_S and f_L, the volume fraction of the large and small bubbles, U_L & U_S, SGV of large and small bubbles, have been obtained for any specific SGV under the condition of stability in other words, minimal dissipation of the energy at the micro-scales [54]. The effective drag co-efficient ratio to the bubble diameter CD/db has been evaluated as a function of SGV using the DBS model and was then combined with the drag force measurement in CFD modeling [55]. Refer to for a comprehensive overview of the DBS model [56]. A set of papers integrating DBS in ALRs hydrodynamics CFD model have been published [50, 54]. Prince and Blanch's coalescence and breakup models have been utilized [57, 58]. The results revealed that when different bubble coalescence and breakup models were utilized, the bubble size distributions and flow regime transitions predicted by PBM were significantly different [59]. To simulate local hydro-dynamics of the gas-liquid-solid 3-phase ALR, the researchers have created a 3-dimensional transient model of the CFD with an embedded MUSIG framework. The breakup and the coalescence of the bubbles have been represented using the Prince and Blanch and the Luo and Svendsen models, respectively. According to the findings, the local transient hydro-dynamic parameters that include the liquid velocities, solid hold-ups, gas hold-ups, and the distribution of bubble size might be predicted with adequate accuracy. When reviewing the work on ALR CFD modeling using various bubble description approaches, it is clear that MUSIG and DBS bubble models are suitable to improve the precision of the simulation, particularly in the case where the local gas hold-up and bubble size distribution have been important. However, in cases where computation resources are restricted, and only average flow parameters are needed, the CFD modeling can be used instead of the MUSIG model.

3.3 Relationships of Closure

The turbulent flow closure laws and the interphase forces, including buoyant force, drag, turbulent dispersion force, and virtual mass force, are also sensitive in CFD simulations of the multi-phase flow. When considering flows in ALRs, different parts of the ALRs have different hydro-dynamic and mixing behavior, complicating the classification [54]. Furthermore, evaluating the effects of isolated forces on the hydro-dynamic parameters in the controlled experimentations has been complicated since the forces behave concurrently, making the selection of adequate closure relationships more complicated. On the other hand, including all of the inter-phase forces in CFD simulation cases is impossible and excessive because of the probability that partial forces could be overlooked. It may seem rational to disregard insignificant forces to save money on computations, but deciding which forces can be ignored at which ALR segment remains a challenge for flow process simulations [54].

3.3.1 Drag Force Closure.

In the case where the bubbles in the surrounding liquid travel at different speeds, drag forces are generated. The drag force is a local slip velocity function between continuous and scattered phases in gas liquid flows. It is typically the most powerful interfacial force [26], as is shown in Eq. (10).

$$F_{l.g}^{D} = \frac{3}{4}\frac{C_D}{d_g}\,\alpha_g\rho_l\left|\vec{V_g} - \vec{V_l}\right|\left(\vec{V_g} - \vec{V_l}\right) \quad (10)$$

However, in low-density foams, Eq. (10) induces unrealistically high drag forces at gas hold-ups approaching 1.0. In addition, by multiplying the local volume fraction of the liquid process, Eq. (11) was proposed as a substitute [60]:

$$F_{l.g}^{D} = \frac{3}{4}\frac{C_D}{d_g}\,\alpha_g\alpha_l\rho_l\left|\vec{V_g} - \vec{V_l}\right|\left(\vec{V_g} - \vec{V_l}\right) \quad (11)$$

The drag coefficient (CD) calculation is important in drag force closure models. According to them [61], the liquid phase's purity affects the drag coefficient, particularly when the liquid phase contains small bubbles or has low surface tension. Since bubbles are deformable, a variety of semi-empirical equations that have been utilized to calculate drag coefficient were suggested for adapting shapes of the ellipse, sphere, and spherical caps. Table 1 includes a list of the typical models of the drag coefficient. However, due to a wide variety of bubble sizes, flow regimes, and shapes, abundant drag, coefficient models don't present a standardized solution, which requires precise establishment of the conditions applicable to every one of the drag coefficient equations.

Table 1: lists typical models of drag coefficients

No	Description of the Model	Application cases
1	$C_D = \frac{24}{R_e}(1+0.15Re^{0.687}) for: Re \le 1000$ $C_D = 0.44 \quad for: Re > 1000$	[43],[62] ,[63]
2	$C_D = \max\left(min\left[\frac{24}{Re}(1+0.15Re^{0.687}).\frac{72}{Re}\right].\frac{8}{3}\frac{Eo}{Eo+4}\right)$	[10]; [64]
3	$C_D = \max\left(\frac{24}{Re}(1+0.15Re^{0.687}).\min(\frac{2}{3}Eo^{0.5}E(\alpha_g).\frac{8}{3}(1-\alpha_g)^2)\right)$ $E(\alpha_g) = \frac{1+17.67f(\alpha_g)^{6/7}}{18.67f(\alpha_g)}.f(\alpha_g) = \frac{\mu_l}{\mu_m}(1-\alpha_g)^{0.5}$	[59];[65];[66]
4	$C_D = \frac{0.622}{1/Eo+0.235}$	[67]
5	$C_D = \frac{2}{3}Ee^{0.5}$	[17]
6	$C_D = \frac{24}{Re}(1+0.15\,Re^{0.687}) + \frac{0.413}{1+16.3Re^{-1.09}} for: Re < 135$ $C_D = 0.95 \quad for: Re > 135$	[5]
7	$C_D = 1 + \frac{24}{Re} + \frac{6}{1+Re^{0.5}}$	[46]
8	$C_D = \frac{4}{3}\frac{g_{ab}}{3v2_t^2}\frac{\rho_l-\rho_g}{\rho_l}$ $U_t = \frac{\mu_g}{\rho_l d_b}Mo^{-0.149}(J-0.857); J = \begin{cases} 0.94H^{0.757}. for: 2 < H < 59.30 \\ 3.42H^{0.441}. for: H > 59.3 \end{cases}$ $H = \frac{4}{3}EoMo^{-0.149}(\frac{\mu_l}{0.0009})^{-0.14} : Mo = \frac{g\mu_l^4(\rho_1-\rho_2)}{\rho_l^2\delta_l^3}$	[24]

3.3.2 Lift Force Closure.

Lift force indicates the interfacial forces that act in a lateral direction perpendicular to primary phase flow in multi-phase flow [25]. The Saffman force, which is induced by shear flow or a gradient of the velocity around bubbles, also Magnus force resulting from forced rotation regarding bubbles in uniform and shear less flow field, are the major mechanisms causing lateral lift forces in ALRs. However, the Saffman force is typically a magnitude order more than the Magnus force in a bubbly flow, rendering the former dominant in ALRs [68]. Due to the low viscosity and the small size of the bubbles in the majority of bubbly flow conditions, the bubble rotation might be ignored; thus, the Magnus force isn't considered in literature [69]. Small bubbles with a positive Saffman lift force coefficient tend to migrate towards the walls in both risers and downcomers, leading to a flatter radial profile of gas hold-up.

In contrast, the large bubbles with negative lift coefficients tend to migrate toward the middle of the cross-section, leading to a center-peak profile of the gas hold-up [4,61]. At 5.8mm as bubble size, the lift force coefficient changes sign in a typical air-water device [70]. Because of its complex position in bubbly flows - bubble deformation, creation of asymmetric wakes, and flows within bubbles - and the lack of precise theoretical explanations, the effects of lift force are often ignored in ALR simulation studies. The researchers usually neglect the impact of lift forces in the simulations of the CFD, considering the numerical calculation stability and lower computation expense [71, 72]. Others believe that lift force has a significant impact on simulation outcomes in areas such as the transversal gas hold-up profile, despite its presence and significance being debatable for practical bubble shapes and sizes [73]. The lift force is determined using Eq. (12) in the available literature:

$$F_{l.g}^{L} = -C_L \rho_l \alpha_g \left(\vec{V_l} - \vec{V_g}\right) \times \left(\nabla \times \vec{V_l}\right) \quad (12)$$

The researchers didn't identify any systematic research on the impacts of the lift force coefficients on the subsequent hydro-dynamic parameters.

3.3.3 Virtual Mass Force Closure

The virtual mass force occurs when the distributed phase is accelerated according to the continuous phase in multi-phase flow. As stated in the user's guide [74], the virtual mass forces are of high importance when scattered phase density is considerably small compared to continuous phase density, like in gas-liquid transient flow. Therefore, Eq. (13) is often used to describe the virtual mass force:

$$F_{l.g}^{V} = C_{VM} \rho_l \alpha_g \left(\frac{D\vec{V_l}}{Dt} - \frac{D\vec{V_g}}{Dt}\right) \quad (13)$$

Drew [75] indicated that the impact of increased mass was observable in the case where slip velocity changed at a high rate. Yet, these oscillations are not resolved in the two-fluid model and are smoothed down throughout the averaging process. As a result, when using a 2-fluid model, the virtual mass force will be ineffective at considerably high computing costs. Sokolichin and Eisenberger [76] also believed that the virtual mass force didn't affect the simulation performance; thus, they recommended that it be ignored, despite its undeniable presence.

3.3.4 Turbulent Dispersion Force Closure

The turbulent dispersion force accounts for inter-phase turbulent momentum transfer, resulting in turbulent diffusion related to the dispersed phase in the continuous phase. Also, the turbulent dispersion force is utilized in the inter-phase drag equation to compensate for the turbulence characteristics' loss. With regard to vertical channel flow, the turbulent dispersion force majorly affects radial gas fraction profiles [41]. Lopez de Bertodano [77] looked at the turbulent dispersion force caused by liquid turbulence, which leads to a more even bubbles' distribution, and derived the simulation eq. by analogy with molecular thermal movements, Eq14:

$$F_l^{td} = -F_g^{td} = C_{TD} \rho_l k_l \nabla \alpha_g \quad (14)$$

Where: -g represents the volume fraction' gradient in the distributed gas phase; k_l represents turbulent kinetic energy in the continuous liquid phase;

C_{TD} represents a turbulent dispersion coefficient that is typically modifiable constant between 0.10 and 0.50. [25]

Simonin and PV [78] looked at bubbles trapped in turbulent eddies in the fluid process and brought from high concentration to lower concentration areas. Eq. (15) is utilized to measure the turbulent dispersion forces:

$$F_l^{td} = -F_g^{td} = C_{TD} k_{l.g} \frac{D_{g.l}^{t}}{\sigma_{TD}} \left(\frac{\nabla \alpha_g}{\alpha_g} - \frac{\nabla \alpha_l}{\alpha_l}\right) \quad (15)$$

Where: - σ_{TD} represents the Prandtl number that has been set to 0.75, $D^{t}_{g.l}$ represent the fluid bubble turbulent dispersion concept connected to distinctive turbulent scales. The derivation can be found in detail in Tavy et al. [5].

Burns [79] has obtained an explicit equation for modeling turbulent dispersion forces by Favre, which averages interphase drag forces based on Eq16:

$$:F_l^{td} = -F_g^{td} = \frac{3}{4} C_D \frac{\alpha_g}{d_g} \left|u_g - u_l\right| \frac{\mu_{t,l}}{Sc_{t,l}} \left(\frac{1}{\alpha_l} + \frac{1}{\alpha_g}\right) \nabla \alpha_g \quad (16)$$

Where: $Sc_{t,l}$: represents turbulent Schmidt number for continuous phase, generally set at 0.90 constant

Talvy et al. [5] have developed a correlation for accounting for turbulent dispersion forces in the frame of the homogeneous turbulence Eq17:

$$F_l^{td} = -F_g^{td} = \rho_l \overline{u_g^t u_l^t} . \nabla \alpha_g \quad (17)$$

The covariance ($u_g u_i$) can be derived from the original source using a series of algebraic equations [13].

3.3.5 Turbulence Closure

Turbulence can be defined as one of the 3D unsteady random motions identified in fluids at moderate-high Reynolds number values that include most industrial flows. Also, the Reynolds Averaged Navier-Stokes (RANS) Eqs. Had been utilized in the 2-fluid model to filter out part or all turbulence continuum leads to a smooth variation regarding averaged velocity and pressure in flow area. Nonetheless, the averaging method provided new unknown terms to conservation equations, like Reynolds stress values, that should be provided through adequate models of turbulence [74]. Therefore, the 2-equation models (k—ω & k—ε models) based on Boussinesq supposition can be considered major turbulence models utilized in realistic flow engineering. In addition, the Reynolds stress has been associated with average velocity gradients in k-ω- and k- ε models through the coefficient of turbulent viscosity (μt), also referred to as effective viscosity (μeff) or eddy viscosity. There are two more transport equations for turbulence kinetic energy k, and either real dissipation rate or turbulence rate of dissipation should be solved for obtaining such coefficient, with the turbulent viscosity evaluated as a k & ω or k & ε function in the following way:

$$u_t = \frac{\rho C_\mu k^2}{\varepsilon} \; or \; u_t = \alpha * \frac{\rho k}{\omega} \tag{18}$$

Where: -Cμ represents a constant, which is commonly fixed at 0.090, α* represents a low Reynolds number correction coefficient equal to 1 for the flows with high Reynolds number values.

Due to its economic character, robustness, capability for predicting wall-bounded turbulent flows, and fair precision, the standard k- ε turbulence model with regard to homogeneous state was majorly utilized [80]. Three turbulent models are used to model multi-phase flow: distributed k- ε-model, mixture k- ε -model, and per phase k- ε turbulence model [74]. Those turbulence models use similar model constants to previous ones, yet they use distinctive equations for accounting for turbulence viscosity [81]. Separate phases, nearly-stratified or stratified multi-phase flows, and phase density ratios of approximately one are covered via the mixture model. Regarding a primary continuous phase that contains a dilute dispersed phase, the dispersed k- ε- model has been found effective. In addition, the per-phase k- ε- turbulence model was considered the most common for multi-phase flows because it is used for solving a group of k as well as ε transport Eqs.

Regarding every one of the phases, they benefit from the majority of computing resources of the 3 models. On the other hand, this model ensures accurate simulation at dominant turbulence transition between the phases, for instance, at high gas void contents [82]. Huang et al. [4] created a 2-fluid 3D steady-state CFD code for IL-ALRs that utilizes a mix k- ε turbulence model to overcome turbulence. The findings showed fair agreement with experimental evidence at correctly presented hydro-dynamic characteristics. Xu et al. [54] utilized the standard mix k- ε turbulence model to predict the liquid velocity in IL-ALR: the forecast has been consistent with experimental results at lower SGV yet underestimated at high SGV. This could be because of the turbulence interactions between the phases, which have been overlooked in k- ε mixture turbulence yet appears at higher SGV. Using distributed k- ε turbulence for simulating transient gas-liquid flows in the ALRs has been proposed in light of the last situation. For instance, Liew et al. [49] utilized a 2-fluid model for simulating the transient 3D ALRs through conducting standard dispersed k-turbulence, which predicted (correctly) the axial liquid velocities as well as the gas hold-ups over a broad SGV range. A few studies proposed modeling turbulence with dispersed k- ε, yet using bubble-induced turbulence as a further source word in ε and k equations, for obtaining more precise modeling results or in a few distinctive application cases. Kantarci et al. [83] utilized the Eulerian 2-fluid model for simulating the bubbly flow in the internal loop airlift column.

Furthermore, just the turbulence equations for the continuous liquid phase have been solved. However, the impact of bubble-induced turbulence on the primary phase has been modeled using a further source terms system. Striba et al. [84] applied the CFD method to simulate the gas liquid dispersion and kinetics regarding removing the ferrous ions from the drinking water through aeration in split rectangular ALRs. In the liquid phase, the stress tensor has been assessed using dispersed k- ε turbulence that accounts for more bubble-induced turbulence and gas dispersion forces. Comparably, with regard to turbulence closure, dispersed k- turbulence was defined elsewhere [46, 51, and 63]. However, the authors were unable to locate works that described per phase k- ε turbulence models for simulating flows in ALRs, because the gas density in the bubbly flow has been low compared with the liquid, which makes separate computations regarding the gas turbulence uneconomic and inessential because of the significant increase in computation resource requirements.

4. Conclusions

The methodology of the simulation of the CFD has provided unparalleled benefits when simulating multi-phase flows in ALRs. CFD is a tool for solving scientific challenges, including flow regime transition research, the acquisition of unmeasurable flow characteristics, and a technological or application pre-requisite for multi-phase flow processes. However, due to the complexity of gas-liquid fluxes, a large amount of theoretical and experimental study is required. The next factious must be taken into account in future works to harness the benefits of numerical simulation effectively:

1) Unlike the CFD model, the mechanism model does not provide extensive local flow parameter data. Before using CFD simulation, it was determined that the flow regime where the reactor is operating should be assessed. More research is needed into the mechanism model, especially the links between flow regimes, bubble features and operational conditions.

2) A few closure relationships, like the impact of shape and bubble size on many interphase powers, are still not simple or systematic.

3) CFD sub-model selection techniques must be standardized, which necessitates the creation of a complete collection regarding the sub-model selection techniques. For example, the bubble definition, frame, and closure relationships models might be evaluated using established selection techniques and characteristics such as SGV, reactor geometry, and flow regimes along with a pre-defined selection flow sheet. Because present work on such problems is either non-existent or insufficient, if

such challenges are properly resolved, the numerical simulation methodology can be highly important in operation optimization and reactor design.

Appendix

Overview of previous work of the model of the CFD for gas-liquid flow in an airlift reactor

Symbols and units:
C_D: drag coefficient
d: diameter, mm.
SGV: superficial gas velocity m^2/s.
V: represents the phase velocity vector.
C_L: the lift coefficient.
CVM: represents the virtual mass coefficient that is commonly set as a constant value which is equal to 0.50 [61, 62].
σ_{TD} : represents Prandtl number that has been set to 0.75.
Sc_{tl}: represents turbulent Schmidt number for continuous phase, generally fixed at 0.90 constant
Greek Letters:-
α: volume fraction ,dimensionless.
Abbreviations:
C_{TD}: the turbulent dispersion coefficient
ALR: air-lift reactor
CARPT: Computer-Automated Radioactive Particle Tracking
CT: sophisticated computed tomography technique
RTD: Residence Time Distribution
PBR: photo bioreactor
E-E: Eulerian-Eulerian model
E-L: Eulerian-Lagrangian model
IL-ALR: - internal loop air-lift reactor
DBS: dual-bubble-size.
PBM: population balance model.
EMMS: energy minimization multi-scale.
D /Dt: - represents the material derivative ;
G:- gas phase ; l :- liquid phase

Acknowledgment

The authors would like to acknowledge the Iraqi government Ministry of Higher Education Iraq & scientific research and The Chemical Engineering department at University of Technology in Baghdad to help the graduate students to get their Master's degree.

Author contribution

All authors contributed equally to this work.

Funding

This research received no specific grant from any funding agency in the public, commercial, or not-for-profit sectors.

Data availability statement

The data that support the findings of this study are available on request from the corresponding author.

Conflicts of interest

The authors declare that there is no conflict of interest.

References

[1] D. J. Pollard, A. P. Ison, P. A. Shamlou, M. D. Lilly. Reactor Heterogeneity with Saccharopolysporaerythraea Airlift Fermentations. Biotechnol. Bioeng., 58 (1998) 453–463. https://doi.org/10.1002/(SICI)1097-0290(19980605)58:5%3C453::AID-BIT1%3E3.0.CO;2-C

[2] J. J. Heijnen,J. Hols, R. G. Van Der Lans, H. L. van Leeuwen, A. Mulder, and R. A. Weltevrede, Simple hydrodynamic model for the liquid circulation velocity in a full-scale two- and three-phase internal airlift reactor operating in the gas recirculation regime, Chem Eng Sci., 52 (1997) 2527-2540. https://doi.org/10.1016/S0009-2509(97)00070-5

[3] M. Y. Christi, Airlift Reactors: Current Technology, Airlift Bioreactors, (1989) 33–86.

[4] Q. Huang, C. Yang, G. Yu, Z.-S. Mao, CFD simulation of hydrodynamics and mass transfer in an internal airlift loop reactor using a steady two-fluid model, Chem. Eng. Sci., 65 (2010) 5527–5536. http://dx.doi.org/10.1016%2Fj.ces.2010.07.021

[5] S. Talvy, A. Cockx, A. Liné, Modeling hydrodynamics of gas–liquid airlift reactor, Aiche J. 53 (2007) 335–353. https://doi.org/10.1002/aic.11078

[6] A. Mirn, A. Gmez, F. Camacho, E M. Grima, Y Chisit,Comparative evaluation of compact photobioreactors for large-scale monoculture of microalgae, 99 (1999). https://doi.org/10.1016/S0168-1656%2899%2900079-6

[7] M. Janssen,Cultivation of microalgae: effect of light / dark cycles on biomass yiel,2002. ISBN: 90-5808-592-9.

[8] H. Luo, M. H. Al-dahhan, Analyzing and Modeling of Photobioreactors by Combining First Principles of Physiology and Hydrodynamics, Missouri Univ. Sci.Technol., 85 (2004) 382-393. https://doi.org/10.1002/bit.10831

[9] H. Dhaouadi, S. Poncin, J.M. Hornut, G. Wild, and P. Oinas, Hydrodynamics of an airlift reactor: experiments and modeling, Chem. Eng. Sci., 51 (1996) 2625–2630. http://dx.doi.org/10.1016/0009-2509(96)00127-3

[10] M. Šimčík, A. Mota, M.C. Ruzicka, A. Vicente, and J. Teixeira, CFD simulation and experimental measurement of gas hold-up and liquid interstitial velocity in internal loop airlift reactor, Chem. Eng. Sci., 66 (2011) 3268–3279. http://dx.doi.org/10.1016/j.ces.2011.01.059

[11] M. Gluz, J. Merchuk, Modified airlift reactors: the helical flow promoters, Chem. Eng. Sci., 51 (1996) 2915–2920. https://doi.org/10.1016/0009-2509(96)00174-1

[12] P.-M. Wang, T.-K. Huang, H.-P. Cheng, Y.-H. Chien, and W.-T. Wu, A modified airlift reactor with high capabilities of liquid mixing and mass transfer, J. Chem. Eng. Jpn., 35 (2002) 354–359. https://doi.org/10.1252/jcej.35.354

[13] T. Zhang, C. Wei, C. Feng, and J. Zhu, A novel airlift reactor enhanced by funnel in- ternals and hydrodynamics prediction by the CFD method, Bioresour. Technol., 104 (2012) 600–607. https://doi.org/10.1016/j.biortech.2011.11.008

[14] M.H. Siegel, and J.C. Merchuk, Mass transfer in a rectangular air-lift reactor: effects of geometry and gas re-circulation, Biotechnol. Bioeng., 32 (1988) 1128–1137. https://doi.org/10.1002/bit.260320906

[15] Ziervogel, G. et al., Climate change and adaptation in African agriculture', Training, 417, 53. Microsoft Word - SEI Rockefeller Africa Climate Report 4April08.doc (environmentportal.in), 2008.

[16] M. Blažej, M. Kiša, J. Markoš, Scale influence on the hydrodynamics of an internal loop airlift reactor, Chem. Eng. Process. Process. Intensif., 43 (2004) 1519–1527. https://doi.org/10.1016/j.cep.2004.02.003

[17] J.M. van Baten, J. Ellenberger, R. Krishna, Hydrodynamics of internal air-lift re- actors: experiments versus CFD simulations, Chem. Eng. Process. Process. Intensif., 42 (2003) 733–742. https://doi.org/10.1016/S0255-2701(02)00076-4

[18] M. Vesvikar, M. Aldahhan, Hydrodynamics Investigation of Laboratory-Scale Internal Gas-Lift Loop Anaerobic Digester using Non-Invasive CAPRT Technique, 1 (2015) 573. https://doi.org/10.1016/j.biombioe.2015.11.014

[19] H.-P. Luo, M.H. Al-Dahhan, Local characteristics of hydrodynamics in draft tube airlift bioreactor, Chem. Eng. Sci., 63 (2008) 3057–3068. https://doi.org/10.1016/j.ces.2008.03.015

[20] H.-P. Luo, M.H. Al-Dahhan, Local gas hold-up in a draft tube airlift bioreactor, Chem. Eng. Sci., 65 (2010) 4503–4510. https://doi.org/10.1016/j.ces.2010.04.037

[21] L. S. Sabri, A. J. Sultan, M. H. Al-Dahhan, Investigating the cross-sectional gas hold-up distribution in a split internal-loop photobioreactor during microalgae culturing using a sophisticated computed tomography (CT) technique, Chem. Eng. Res. Des., 149 (2019) 13–33. https://doi.org/10.1016/j.cherd.2019.06.017

[22] L. S. Sabri, A. J. Sultan, M. H. Al-Dahhan, Split internal-loop photobioreactor for Scenedesmus sp. microalgae: Culturing and hydrodynamics, Chin. J. Chem. Eng., 33 (2021) 236-248. https://doi.org/10.1016/j.cjche.2020.07.058

[23] R.F. Mudde, H.E.A. Van Den Akker, 2D and 3D simulations of an internal airlift loop reactor on the basis of a two-fluid model, Chem. Eng. Sci., 56 (2001) 6351–6358. https://doi.org/10.1016/S0009-2509(01)00222-6

[24] H.-P. Luo, M.H. Al-Dahhan, Verification and validation of CFD simulations for local flow dynamics in a draft tube airlift bioreactor, Chem. Eng. Sci., 66 (2011) 907–923. https://doi.org/10.1016/j.ces.2010.11.038

[25] G. V. Tagliaferro, H. J. IzárioFilho, A. K. Chandel, S. S. Silva, M. B. Silva, J. C. Santos, Continuous cultivation of Chlorella minutissima 26a in landfill leachate-based medium using concentric tube airlift photobioreactor, Algal Research, 41 (2019). https://doi.org/10.1016/j.algal.2019.101549

[26] J. Behin, Modeling of modified airlift loop reactor with a concentric double-draft tube, Chem. Eng. Res. Des. 88 (2010) 919–927. https://doi.org/10.1016/j.cherd.2010.01.004

[27] O. O. Olaofe, K. A. Buist, N. G. Deen, .M. A. Van der Hoef, J. A. M. Kuipers, Simulation of particle mixing and segregation in disperse gas fluidized beds, Chem. Eng. Sci., 108 (2014) 258-269. https://doi.org/10.1016/j.ces.2014.01.009

[28] A. Couvert, M. Roustan, P. Chatellier, Two-phase hydro-dynamic study of a rectangular air-lift loop reactor with an internal baffle, Chem. Eng. Sci., 54 (1999) 5245–5252. https://doi.org/10.1016/S0009-2509(99)00246-8

[29] J.C. Merchuk, M.H. Siegel, Air-lift reactors in chemical and biological technology, J. Chem. Technol. Biotechnology. 41 (1988) 105–120. https://doi.org/10.1002/jctb.280410204

[30] Y.Z. Li, Y.L. He, D.G. Ohandja, J. Ji, J.F. Li, T. Zhou, Simultaneous nitrification–denitrification achieved by an innovative internal-loop airlift MBR: comparative study, Bioresource. Technol., 99 (2008) 5867–5872. https://doi.org/10.1016/j.biortech.2007.10.001

[31] T. Zhang, C. Wei, A new developed airlift reactor integrated settling process and its application for simultaneous nitrification and denitrification nitrogen removal, Sci. World J., 2013 (2013)7. https://doi.org/10.1155/2013/345725

[32] L. Meng, Y. Bando, M. Nakamura, Dissolved oxygen distribution in a rectangular airlift bubble column for biological nitrogen removal, J. Chem. Eng. Jpn. 37 (2004) 1005–1011. https://doi.org/10.1252/jcej.37.1005

[33] L. Meng, N. Tsuno, Y. Bando, M. Nakamura, Enhancement of nitrogen removal in a rectangular airlift bubble column having aerobic and anaerobic regions by adding an immobilizing carrier, J. Chem. Eng. Jpn.,37 (2004) 399–405. https://doi.org/10.1252/jcej.37.399

[34] Q. Meng, F. Yang, L. Liu, F. Meng, Effects of COD/N ratio and DO concentration on simultaneous nitrification and denitrification in an airlift internal circulation membrane bioreactor, J. Environ. Sci., 20 (2008) 933–939. https://doi.10.1016/s1001-0742(08)62189-0

[35] E. García-Calvo, A. Rodríguez, A. Prados, J. Klein, A fluid dynamic model for three-phase airlift reactors, Chem. Eng. Sci., 54 (1999) 2359–2370. https://doi.org/10.1016/S0009-2509(98)00302-9

[36] S. Hutmacher 'Sensitivity Study on Modeling an Internal Airlift Loop Reactor Using a Steady 2D Two-Fluid Model' chem. Eng. Tech., (2008) 1790–1798. https://doi.org/10.1002/ceat.200700278

[37] J.B. Joshi, Computational flow modelling and design of bubble column reactors, Chem. Eng. Sci., 56 (2001) 5893–5933. https://doi.org/10.1016/S0009-2509(01)00273-1

[38] P. Chen, J. Sanyal, M. P. Dudukovi, Numerical simulation of bubble columns flows: effect of different breakup and coalescence closures, Chem.Eng.Sci., 60 (2005) 1085–1101. https://doi.org/10.1016/j.ces.2004.09.070

[39] H. A. Jakobsen, C. A. Dorao, Modeling of Bubble Column Reactors: Progress and Limitations, Ind. Eng. Chem. Res., 44 (2005)5107–5151. https://doi.org/10.1021/ie049447x

[40] D. Lucas, E. Krepper, H.-M. Prasser, use of models for lift, wall and turbulent dispersion forces acting on bubbles for poly-disperse flows, Chem. Eng. Sci., 62 (2007) 4146–4157. https://doi.org/10.1016/j.ces.2007.04.035

[41] J. M. Baten, J. Ellenberger, R. Krishna, Hydrodynamics of internal air-lift reactors: experiments versus CFD simulations, Chem. Eng. Process. Process. Intensif., 42 (2003) 733–742. https://doi.org/10.1016/S0255-2701(02)00076-4

[42] Q.S. Huang, C. Yang, G.Z. Yu, Z.S. Mao, 3-d simulations of an internal airlift loop reactor using a steady two-fluid model, Chem. Eng. Technol., 30 (2007) 870–879. https://doi.org/10.1002/ceat.200700038

[43] S.B. Pawar, CFD analysis of flow regimes in airlift reactor using Eulerian- Lagrangian approach, Can. J. Chem. Eng. ,95 (2016) 420–431. https://doi.org/10.1002/cjce.22696

[44] S.M. Teli, C. Mathpati, Experimental and Numerical Study of Gas-Liquid Flow in a Sectionalized External-Loop Airlift Reactor, Chin. J. Chem. Eng., 32 (2021) 39-60.https://doi.org/10.1016/j.cjche.2020.10.023

[45] Z. Qiao, et al. PVAm–PIP/PS composite membrane with high performance for CO2/N2 separation, AIChE J., 59 (2012) 215–228. https://doi.org/10.1002/aic.13781

[46] N.T. Padial, W.B. VanderHeyden, R.M. Rauenzahn, S.L. Yarbro, Three-dimensional simulation of a three-phase draft-tube bubble column, Chem. Eng. Sci., 55 (2000) 3261–3273. https://doi.org/10.1016/S0009-2509(99)00587-4

[47] V. Michele, D.C. Hempel, Liquid flow and phase hold-up—measurement and CFD modeling for two-and three-phase bubble columns, Chem. Eng. Sci., 57 (2002) 1899–1908. https://doi.org/10.1016/S0009-2509(02)00051-9

[48] Y. Liew Shi, J. Gimbun, CFD simulation on the hydrodynamics in Gas-Liquid airlift reactor, Chem. Prod. Process. Model., 12 (2017) 20170030. https://doi.org/10.1515/cppm-2017-0030

[49] M. Yang, D. Yu, M. Liu, L. Zheng, X. Zheng, Y. Wei, F. Wang, Y. Fan, Optimization of MBR hydrodynamics for cake layer fouling control through CFD simulation and RSM design, Bioresour. Technol., 227 (2017) 102–111. https://doi.org/10.1016/j.biortech.2016.12.027

[50] M. Mohajerani, M. Mehrvar, F. Ein-Mozaffari, CFD analysis of two-phase turbulent flow in internal airlift reactors, Can. J. Chem. Eng., 90 (2012) 1612–1631. https://doi.org/10.1002/cjce.20674

[51] N. Qi, K. Zhang, G. Xu, Y. Yang, H. Zhang, CFD-PBE simulation of gas-phase hydrodynamics in a gas-liquid-solid combined loop reactor, Pet. Sci., 10 (2013) 251–261. https://doi.org/10.1007/s12182-013-0274-5

[52] J.H. Li, Multi-scale Modeling and Method of Energy Minimization for Particle- fluid Two-phase Flow. PhD Thesis, Institute of Chemical Metallurgy, Academia Sinica, 1987.

[53] T. Xu, X. Jiang, N. Yang, J. Zhu, CFD simulation of internal-loop airlift reactor using EMMS drag model, Particuology,19 (2015) 124–132. https://doi.org/10.1016/j.partic.2014.04.016

[54] N. Yang, Z. Wu, J. Chen, Y. Wang, J. Li, Multi-scale analysis of gas–liquid inter- action and CFD simulation of gas–liquid flow in bubble columns, Chem. Eng. Sci., 66 (2011) 3212–3222. https://doi.org/10.1016/j.ces.2011.02.029

[55] N. Yang, J. Chen, H. Zhao, W. Ge, J. Li, Explorations on the multi-scale flow structure and stability condition in bubble columns, Chem. Eng. Sci., 62 (2007) 6978–6991. https://doi.org/10.1016/j.ces.2007.08.034

[56] Z. Deng, et al. Gas hold-up, bubble behavior and mass transfer in a 5m high internal-loop airlift reactor with non-Newtonian fluid, Chem. Eng. J., 160 (2010) 729–737. https://doi.org/10.1016/j.cej.2010.03.078

[57] T. Wang, J. Wang, Y. Jin, Population balance model for gas−Liquid flows: in- fluence of bubble coalescence and breakup models, Ind. Eng. Chem. Res., 44 (2005) 7540–7549. https://doi.org/10.1021/ie0489002

[58] X. Jia, J. Wen, H. Zhou, W. Feng, Q. Yuan, Local hydrodynamics modeling of a gas–liquid–solid three-phase bubble column, Aiche J., 53 (2007) 2221–2231. https://doi.org/10.1002/aic.11254

[59] S. Geng, et al. Hydrodynamics and mass transfer in a slurry external airlift loop reactor integrating mixing and separation, Chem. Eng. J., 211 (2020) 115294. https://doi.org/10.1016/j.ces.2019.115294

[60] A. Tomiyama, H. Tamai, I. Zun, S. Hosokawa, Transverse migration of single bubbles in simple shear flows, Chem. Eng. Sci., 57 (2002) 1849–1858. https://doi.org/10.1016/S0009-2509(02)00085-4

[61] Z. Naumann, L. Schiller, A drag coefficient correlation, Z Ver Deutsch Ing. 77 (1935) 318–323.

[62] R. Bannari, A. Bannari, B. Selma, P. Proulx, Mass transfer and shear in an airlift bioreactor: using a mathematical model to improve reactor design and performance, Chem. Eng. Sci., 66 (2011) 2057–2067. https://doi.org/10.1016/j.ces.2011.01.038

[63] A. Tomiyama, I. Kataoka, I. Zun, T. Sakaguchi, Drag coefficients of single bubbles under normal and Micro gravity conditions, Jsme Int. J. Ser. B., 41 (1998) 472–479. https://doi.org/10.1299/jsmeb.41.472

[64] Kolev N., Multiphase Flow Dynamics 2: Thermal and Mechanical Interactions, Springer, Berlin, Germany, 20052005, 1994.

[65] X. Wang, X. Jia, J. Wen, Transient modeling of toluene waste gas biotreatment in a gas–liquid airlift loop reactor, Chem. Eng. J., 159 (2010) 1–10. https://doi.org/10.1016/j.cej.2010.02.006

[66] M.K. Moraveji, B. Sajjadi, M. Jafarkhani, R. Davarnejad, Experimental investigation and CFD simulation of turbulence effect on hydro-dynamic and mass transfer in a packed bed airlift internal loop reactor, Int. Commun. Heat Mass Transf, 38 (2011) 518–524. https://doi.org/10.1016/j.icheatmasstransfer.2010.12.033

[67] J. Liao, T. Ziegenhein, R. Rzehak, Bubbly flow in an airlift column: a CFD study, J. Chem. Technol. Biotechnol.,91 (2016) 2904–2915. https://doi.org/10.1002/jctb.4917

[68] Z. Yu, B. Zhu, S. Cao, Interphase force analysis for air-water bubbly flow in a multi-phase rotodynamic pump, Eng. Comput. (Swansea), 32 (2015) 2166–2180. https://doi.org/10.1108/EC-10-2014-0210

[69] D. Lucas, E. Krepper, H.-M. Prasser, Prediction of radial gas profiles in vertical pipe flow on the basis of bubble size distribution, Int. J. Therm. Sci., 40 (2001) 217–225. https://doi.org/10.1016/S1290-0729(00)01211-4

[70] R.S. Oey, R.F. Mudde, L.M. Portela, H.E.A. van den Akker, Simulation of a slurry airlift using a two-fluid model, Chem. Eng. Sci., 56 (2001) 673–681. https://doi.org/10.1016/S0009-2509(00)00275-X

[71] F. Kerdouss, A. Bannari, P. Proulx, R. Bannari, M. Skrga, Y. Labrecque, Two-phase mass transfer coefficient prediction in stirred vessel with a CFD model, Comput. Chem. Eng., 32 (2008) 1943–1955. https://doi.org/10.1016/j.compchemeng.2007.10.010

[72] A. Sokolichin, G. Eigenberger, A. Lapin, Simulation of buoyancy driven bubbly flow: established simplifications and open questions, Aiche J., 50 (2004) 24–45. https://doi.org/10.1002/aic.10003

[73] Fluent A., 12.0 User's Guide, Ansys Inc, 2009.

[74] D.A. Drew, Mathematical modeling of two-phase flow, Annu. Rev. Fluid Mech., 15 (1983) 261–291. https://doi.org/10.1146/annurev.fl.15.010183.001401

[75] R. Rzehak, T. Ziegenhein, S. Kriebitzsch, E. Krepper, D. Lucas, Unified modeling of bubbly flows in pipes, bubble columns, and airlift columns, Chem. Eng. Sci., 157 (2017) 147–158. https://doi.org/10.1016/j.ces.2016.04.056

[76] M.A. Lopez de Bertodano, Two fluid model for two-phase turbulent jets, Nucl. Eng. Des., 179 (1998) 65–74. https://doi.org/10.1016/S0029-5493(97)00244-6

[77] O. Simonin, P. V, Modelling of turbulent two-phase jets loaded with discrete particles, Phenomena in Multiphase Flows, 1990 (1990) 259–269. https://doi.org/10.1115/1.3124445

[78] A.D.B. Burns, drag model for turbulent dispersion in eulerian multi-phase flows, Proc 5th International Conference of Multiphase Flow ,2004.

[79] L. Chen, Z. Bai, CFD simulation of the hydrodynamics in an industrial scale cy- clohexane oxidation airlift loop reactor, Chem. Eng. Res. Des., 119 (2017) 33–46. https://doi.org/10.1016/j.cherd.2017.01.008

[80] J. Gimbun, Assessment of the Turbulence Models for Modelling of Bubble Column, J. Inst. Eng. Malays., 70 (2010) 57-64.

[81] J.P. Bitog, I.B. Lee, C.G. Lee, K.S. Kim, H.S. Hwang, S.W. Hong, I.H. Seo, K.S. Kwon, E. Mostafa, Application of computational fluid dynamics for modeling and designing photobioreactors for microalgae production: a review, Comput. Electron. Agric., 76 (2011) 131–147. https://doi.org/10.1016/j.compag.2011.01.015

[82] N. Kantarci, F. Borak, and K. O. Ulgen, Bubble column reactors. Process Biochemistry, 40 (2005) 2263–2283. https://doi.org/10.1016/j.procbio.2004.10.004

[83] Y. Stiriba, B. Gourich, C. Vial, Numerical modeling of ferrous iron oxidation in a split-rectangular airlift reactor, Chem. Eng. Sci., 170 (2017) 705–719. https://doi.org/10.1016/j.ces.2017.03.047